

The second *Konus-Wind* catalog of short gamma-ray bursts

D. S. Svinkin, D. D. Frederiks, R. L. Aptekar, S. V. Golenetskii, V. D. Pal'shin,

Ph. P. Oleynik, A. E. Tsvetkova, M. V. Ulanov,

Ioffe Institute, Politekhmicheskaya 26, St. Petersburg, 194021, Russia

T. L. Cline¹,

NASA Goddard Space Flight Center, Greenbelt, MD 20771, USA

and

K. Hurley

Space Sciences Laboratory, University of California, 7 Gauss Way, Berkeley, CA

94720-7450, USA

Received _____; accepted _____

¹Emeritus

ABSTRACT

In this catalog, we present the results of a systematic study of 295 short gamma-ray bursts (GRBs) detected by *Konus-Wind* (KW) from 1994 to 2010. From the temporal and spectral analyses of the sample, we provide the burst durations, the spectral lags, the results of spectral fits with three model functions, the total energy fluences and the peak energy fluxes of the bursts. We discuss evidence found for an additional power-law spectral component and the presence of extended emission in a fraction of the KW short GRBs. Finally, we consider the results obtained in the context of the Type I (merger-origin) / Type II (collapsar-origin) classifications.

Subject headings: gamma-ray burst: general — catalogs

1. INTRODUCTION

Gamma-ray bursts (GRBs) can be divided into two distinct morphological classes based on the properties of the observed gamma-ray emission: short/hard GRBs, which typically last less than 2 s, have hard prompt-emission spectra and negligible spectral lag, and long/soft GRBs which last typically longer than 2 s, have softer spectra and non-negligible spectral lag (Mazets et al. 1981; Kouveliotou et al. 1993; Norris et al. 2000; Norris & Bonnell 2006).

It is believed that the physical origins of long/soft and short/hard bursts are different. Short/hard GRBs are thought to be the results of mergers of binary compact objects (so called Type I GRBs), such as two neutron stars or a neutron star and a black hole (see, e.g. Berger 2014 and references therein), while long/soft (Type II GRBs), which are occasionally accompanied by supernovae, originate from the core collapse of massive stars (see Zhang et al. 2009 for more information on the Type I/II classification scheme).

The *Konus-Wind* gamma-ray burst spectrometer (hereafter KW, Aptekar et al. 1995) has observed ~ 2500 GRBs, with ~ 400 of them being short GRBs, in the period from launch in 1994 to 2015. Here, we present the second KW short GRB catalog which provides spectral and temporal characteristics of one of the largest short GRB samples to date over a broad energy band. Specifically, the catalog covers GRBs occurring during the period from 1994 November to 2010 December and includes about twice the number of bursts as the first *Konus* catalog of short GRBs¹ (Mazets et al. 2002).

We start with a description of the KW detectors in Section 2. In Section 3 we provide details of the KW short GRB sample. We describe the analysis procedures in Section 4 and present the results in Section 5. Finally, in Section 6 we conclude with a summary.

¹The data are available at <http://www.ioffe.ru/LEA/shortGRBs/Catalog/>

2. KONUS-WIND

KW consists of two identical NaI(Tl) detectors S1 and S2, each with 2π field of view. The detectors are mounted on opposite faces of the rotationally stabilized *Wind* spacecraft, such that one detector (S1) points towards the south ecliptic pole, thereby observing the south ecliptic hemisphere, while the other (S2) observes the north ecliptic hemisphere. Each detector has an effective area of $\sim 80\text{--}160\text{ cm}^2$ depending on the photon energy and incident angle. The nominal energy range of gamma-ray measurements covers the incident photon energy interval from 13 keV up to 10 MeV.

In interplanetary space far outside the Earth’s magnetosphere, KW has the advantages over Earth-orbiting GRB monitors of continuous coverage, uninterrupted by Earth occultation, and a steady background, undistorted by passages through the Earth’s trapped radiation, and subject only to occasional solar particle events. The *Wind* distance from Earth as a function of time is presented in Pal’shin et al. (2013). The maximum distance was $\sim 7\text{ lt-s}$ in 2002 January and May; since 2004 *Wind* has been in a Lissajous orbit at the L_1 libration point of the Sun-Earth system at a distance of $\sim 5\text{ lt-s}$.

The instrument has two operational modes: waiting and triggered. While in the waiting mode, the count rates are recorded in three energy windows G1 (13–50 keV), G2 (50–200 keV), and G3 (200–760 keV) with 2.944 s time resolution. When the count rate in the G2 window exceeds a $\approx 9\sigma$ threshold above the background on one of two fixed time-scales, 1 s or 140 ms, the instrument switches into the triggered mode. In the triggered mode, the count rates in the three energy windows are recorded with time resolution varying from 2 ms up to 256 ms. These time histories, with a total duration of $\sim 230\text{ s}$, also include 0.512 s of pre-trigger history. Spectral measurements are carried out, starting from the trigger time T_0 , in two overlapping energy intervals, 13–760 keV and 160 keV–10 MeV, with 64 spectra being recorded for each interval over a 63-channel, pseudo-logarithmic energy

scale. The first four spectra are measured with a fixed accumulation time of 64 ms in order to study short bursts. For the subsequent 52 spectra, an adaptive system determines the accumulation times, which may vary from 0.256 to 8.192 s depending on the current count rate in the G2 window. The last 8 spectra are obtained for 8.192 s each. As a result the minimum duration of spectral measurements is 79.104 s, and the maximum is 491.776 s.

The detector response matrix (DRM), which is a function only of the energy and incident angle, was computed using the GEANT4 package (Agostinelli et al. 2003). The detailed description of the instrument response calculation is presented in Terekhov et al. (1998). The latest version of the DRM contains responses calculated for 255 photon energies between 5 keV and 26 MeV on a quasi-logarithmic scale for incident angles from 0° to 90° with a step of 5° . The energy scale is calibrated in-flight using the 1460 keV line of ^{40}K and the 511 keV annihilation line.

The gain of the detectors has slowly decreased during the long period of operation. The instrumental control of the gain became non-functional in 1997 and the spectral range changed to 25 keV–18 MeV for the S1 detector and to 20 keV–15 MeV for the S2 detector, from the original 13 keV–10 MeV. The spectral resolution of the detectors ($\Delta E/E$) did not change significantly during the mission, with an upper limit, estimated at $E = 1460$ keV, of $\Delta E/E \lesssim 10\%$ (FWHM) for the whole period of monitoring. The corresponding resolution loss is less than a factor of 1.5 compared to the ground-based calibrations ($\Delta E/E \approx 6.5\%$ at 1460 keV, FWHM).

For all short GRBs we use a standard KW dead time (DT) correction procedure for light curves (with a DT of a few microseconds) and spectra (with a DT of ~ 42 microseconds). Although the photon flux for some short GRBs is very high (up to $\sim 10^5$ counts s^{-1}), this procedure is still applicable; no additional correction, which was used, e.g., in an analysis of the KW detection of the 1998 August 27 giant flare from SGR 1900+14, is required

(details of these simulations and the KW dead-time correction procedures can be found in Mazets et al. 1999). Also, at high count rates, a pile-up effect in the analog electronics can distort the low-energy part of the KW instrumental spectra. Our simulations show that, for the bright, hard bursts in our sample, the distorted energy range is limited to $<50\text{--}150$ keV and lies well below the peak energies of the spectra. Accordingly, we found that the exclusion of the potentially distorted channels from spectral fits of the brightest short GRBs results in model parameter changes within the fit uncertainties.

The consistency of the KW spectral parameters with those obtained in other GRB experiments was verified by a cross-calibration with *Swift*-BAT and *Suzaku*-WAM (Sakamoto et al. 2011a), and in joint spectral fits with *Swift*-BAT (Krimm et al. 2006; Roming et al. 2006; Starling et al. 2009) and *Fermi*-GBM (e.g., Lipunov et al. 2016). It was shown that the difference in the spectrum normalization between KW and these instruments is $\lesssim 20\%$ in joint fits.

3. THE SHORT GRB SAMPLE

Between 1994 November and 2010 December, KW detected 1939 GRBs in the triggered mode, 295 of which were classified as short-duration GRBs or short bursts with extended emission (EE). The classification (Svinkin et al., in prep.) was based on the T_{50} duration distribution. T_{90} and T_{50} are the time intervals which contain from 5% to 95% (T_{90}) and from 25% to 75% (T_{50}) of the total burst count fluence (see, e.g., Kouveliotou et al. 1993). In this work, these durations are calculated in the G2+G3 band (nominal bounds 50–760 keV) unless stated explicitly. Using an unbiased sample of 1168 KW GRBs we adopted $T_{50} = 0.6$ s as the boundary between short and long KW GRBs. The instrument trigger criteria cause undersampling of faint short bursts relative to faint long bursts, so this subsample of fairly bright (in terms of peak count rate in the KW trigger energy band)

bursts has been chosen for the purpose of classification.

Although the aim of this work is to report on all KW GRBs that meet the short GRB criterion, the results of a more sophisticated classification of the selected GRBs, which accounts for the burst spectral hardness and its duration (Svinkin et al., in prep.), may be essential for future analysis. The burst spectral hardness (HR_{32}) was calculated using the ratio of counts in the G3 and G2 bands accumulated during the burst duration T_{100} . The calculation of HR_{32} takes into account the gain drift effect. The rates expected in the nominal G2 and G3 energy bands (as given in Section 2) were estimated using the best fit to the burst count spectrum with the CPL function (see Section 4 for the CPL spectral model definition).

The burst types were derived using a method similar to that described in Horváth et al. (2010) and are as follows: I (merger-origin), II (collapsar-origin), I/II (the type is uncertain). The following correspondence between the short/hard burst indicator function $I(T_{50}, \text{HR}_{32})$ (see eq. 5 in Horváth et al. 2010) and the Type was used: $I > 0.9$ — Type I, $0.1 < I < 0.9$ — Type I/II, $I < 0.1$ — Type II. The classification of short GRBs with extended emission (see Section 5.4) was based on the initial pulse parameters and the types are as follows: Iee (type I which shows extended emission, EE), and Iee/II (the type is uncertain: Iee or II). The classification results are shown in Figure 1.

Along with the Type I–II classification we report the spectral lags (τ_{lag}) for bursts in our sample. The spectral lag is a quantitative measure of spectral evolution often seen in long GRBs, when the emission in a soft detector band peaks later relative to a hard band. It was also shown that short GRBs with and without EE have negligible spectral lag (Norris & Bonnell 2006; Norris et al. 2001). Thus, the spectral lag can be used as an additional classification parameter. We calculated τ_{lag} for three pairs of the KW light curves (G2 and G1, $\tau_{\text{lag}21}$; G3 and G2, $\tau_{\text{lag}32}$; and G3 and G1, $\tau_{\text{lag}31}$) using a cross-correlation

method similar to that described in Norris et al. (2000). Details and examples of lag estimations for KW bursts will be given in Svinkin et al. (in prep).

KW has only coarse localization capability on its own, which is crucial for the GRB spectral analyses. In cases where the position of a GRB is not available from an instrument with imaging capabilities (e.g. *Swift*-BAT), the source localization can be derived using InterPlanetary network triangulation (Hurley et al. 2013). The localizations of 296 KW short GRBs detected between 1994 November and 2010 December can be found in (Pal’shin et al. 2013).

Table 1 lists the 295 KW short GRBs. The first column gives the burst designation in the form “GRBYYYYMMDD_Tsssss”, where YYYYYMMDD is the burst date, and sssss is the KW trigger time T_0 (UT) truncated to integer seconds (note that due to *Wind*’s large distance from Earth, this trigger time can differ by up to ~ 7 s from the Earth-crossing time; see Pal’shin et al. 2013). The second column gives the KW trigger time in the standard time format. The “Name” column specifies the GRB name as provided in the Gamma-ray Burst Coordinates Network circulars², if available. The “Detector” column specifies the triggered detector. The next column provides the angle between the GRB direction and the detector axis (the incident angle). The last column contains localization-specific notes.

Our sample contains 19 GRBs with incident angles close to, but slightly greater, than 90° . In these cases we use an incident angle of 90° to calculate the detector response. The positions of three weak bursts, GRB19990831_T41835, GRB20010420_T30786, and GRB20080321_T23721, cannot be constrained to better than an ecliptic hemisphere, so for these GRBs we use an incident angle of 60° .

²http://gc.nas.nasa.gov/gcn3_archive.html

4. SPECTRAL ANALYSIS

A typical KW short GRB spectrum is a subset of the four 64-ms spectra measured from T_0 up to $T_0 + 0.256$ s. The background spectrum for bursts without EE was usually taken from $T_0 + 25$ s with an accumulation time of about 100 s. For about 25% of the bursts, a major fraction of the counts was accumulated before the trigger, in the time interval not covered by the multichannel spectra. For these bursts, a three-channel spectrum, constructed from the light curve counts, is used for the analysis, accumulated over the whole burst duration T_{100} . The spectral sample contains 214 multichannel time-integrated spectra and 79 three-channel spectra. Due to low counting statistics of the majority of our short GRBs we typically use a time-integrated spectrum to calculate both the total energy fluence (S) and the peak energy flux (F_{peak}). Only for 18 fairly intense GRBs from our sample was it possible to derive F_{peak} from a spectrum covering a narrow time interval near the peak count rate.

We chose three spectral models to fit the spectra of GRBs from our sample. These models were a power law (PL), Band’s GRB function (BAND), and an exponential cutoff power-law (CPL). The details of each model are presented below.

The power law model:

$$f_{\text{PL}} \propto E^\alpha \quad (1)$$

The exponentially cutoff power law:

$$f_{\text{CPL}} \propto E^\alpha \exp\left(-\frac{E(2+\alpha)}{E_p}\right) \quad (2)$$

Band’s GRB function (Band et al. 1993):

$$f_{\text{BAND}} \propto \begin{cases} E^\alpha \exp\left(-\frac{E(2+\alpha)}{E_p}\right) & E < (\alpha - \beta)E_p/(2 + \alpha) \\ E^\beta \exp(\beta - \alpha) \left[\frac{(\alpha - \beta)E_p}{(2 + \alpha)}\right] & E \geq (\alpha - \beta)E_p/(2 + \alpha) \end{cases} \quad (3)$$

Where E_p is the peak energy of the EF_E spectrum.

4.1. Multichannel spectra

The spectral analysis of bursts with multichannel spectra was performed using **XSPEC** v. 12.8.0 (Arnaud 1996). The χ^2 statistic was used in the model fitting process as a figure of merit to be minimized. The spectral channels were grouped to have a minimum of 10 counts per channel to ensure the validity of the χ^2 statistic. We use a model energy flux in the 10 keV–10 MeV band as the model normalization during fit. The flux was calculated using the **cflux** convolution model in **XSPEC**. The parameter errors were estimated using the **XSPEC** command **error** based on the change in fit statistic ($\Delta\chi^2 = 2.706$) which corresponds to 90% CL.

We fit the three model functions described above to each multichannel spectrum. The most preferred model (the best-fit model) was chosen based on the difference in χ^2 . The criterion for accepting a model with a single additional parameter is a change in χ^2 of at least 5 with the chance probability for achieving this difference of ≈ 0.025 . We found that this threshold is preferred, for our sample, over the frequently-used $\Delta\chi^2 \geq 6$ because it nearly halves the number of divergent PLs as best-fit models which is crucial when the burst energetics are considered.

4.2. Three-channel spectral analysis

The 79 three-channel spectra were fitted with PL and CPL using a custom-built routine and the confidence limits for the parameters were estimated via the bootstrap approach.

For the purpose of testing the procedure we compared results of the multichannel and

three-channel spectral analysis for the sample of the 214 GRBs with multichannel spectra. For each burst we constructed a three-channel spectrum accumulated over the interval of measurement of the multichannel spectrum. Then we compared parameters of the model that best fits the multichannel spectrum with the parameters of the same model fitted to the three-channel spectrum. In the case of PL the resulting photon indices are consistent between the two types of spectral analysis. For CPL we found that the α values are also generally consistent between the three-channel and multichannel spectra. The same is true for E_p but only when its value is located within the three-channel analysis range (i.e. $\lesssim 1$ MeV), otherwise, the latter method results in an overestimated, poorly constrained E_p . This demonstrates that KW is capable of producing accurate spectral parameter and energetics estimates even when multichannel spectral data are not available.

Since the CPL fit to a three-channel spectrum has zero degrees of freedom (and, in the case of convergence, $\chi^2_{\text{CPL}} = 0$), the best-fit model cannot be easily chosen between PL and CPL on the basis of the $\Delta\chi^2 \geq 5$ criterion. So, in order not to overestimate the burst energetics, we decided to use the CPL model flux to calculate S and F_{peak} for the GRBs for which the three-channel CPL fit results in an E_p constrained from below.

5. RESULTS

5.1. Temporal characteristics and Type I–II classification

Table 2 contains the burst durations, the spectral lags, and classification. The first column gives the burst designation. The following four columns contain the start of the T_{100} interval t_0 (relative to T_0), T_{100} , T_{90} and T_{50} . The errors are given at the 1σ confidence level (CL). For two GRBs (GRB19960325_T69892 and GRB19980614_T31854) T_{90} and T_{50} were calculated in the G2 energy range (nominal bounds 50–200 keV) because of gaps in

the G3 light curve, and these GRBs were excluded from the spectral analyses. The next column gives the Type I–II classification and the last three columns contain $\tau_{\text{lag}21}$, $\tau_{\text{lag}32}$, and $\tau_{\text{lag}31}$. A positive τ_{lag} corresponds to the delay of the softer emission. The lags are provided for bursts having signal-to-noise ratio $\geq 8\sigma$ in the corresponding light curves binned to ≤ 64 ms resolution. Most of the Type I bursts have $\tau_{\text{lag}} < 25$ ms (see Figure 2), while bursts of types I/II and II tend to have long $\gtrsim 100$ ms. For the bursts with EE, the durations and lags in Table 2 are given for the short initial pulse only.

5.2. Spectral parameters

Table 3 provides the results of the multichannel spectral analysis for the 214 time-integrated spectra and the 18 spectra near the peak count rate. For the time-integrated spectra the statistics of the best-fit models are as follows: CPL — 201 GRBs, BAND — 9 GRBs, and PL — 4 GRBs. Along with the best-fit model parameters we present the results for the models whose parameters are constrained (hereafter, GOOD models). For the CPL and BAND GOOD models we require both α and E_p errors to be constrained, and, for the BAND model, $\beta > -4$. To reject models with apparent systematics in the fit residuals, we also require a null hypothesis probability $P > 10^{-6}$ for the fit. The ten columns in Table 3 contain the following information: (1) the burst designation (see Table 1); (2) the spectrum type, where ‘i’ indicates that the spectrum is time-integrated and is used to calculate S , ‘p’ means that the spectrum is measured near the peak count rate (and is used to calculate F_{peak}), or both ‘i,p’; columns (3) and (4) contain the spectrum start time T_{start} (relative to T_0) and its accumulation time ΔT ; (5) GOOD models for each spectrum; (6)–(8) low-energy spectral index α , high-energy spectral index β , and E_p ; (9) normalization (energy flux in 10 keV–10 MeV band); (10) χ^2/dof along with the null hypothesis probability P . In cases where the lower limit for β is not constrained, the value of $(\beta_{\text{min}} - \beta)$ is provided instead,

where $\beta_{\min} = -10$ is the lower limit for the fits. In total, the table contains results for 473 fits of time-integrated spectra with different models (210 — CPL, 117 — BAND, and 146 — PL).

Table 4 contains results obtained from fits of the 79 three-channel spectra. For all but one of these GRBs we present the CPL model parameters and, for GRB19961113_T80522, for which E_p is not constrained, the PL fit results ($\chi^2 = 1.6 \times 10^{-4}$) are provided. A nonzero χ^2_{CPL} was obtained only for two out of the 78 bursts: GRB20000623_T03887 ($\chi^2 = 0.4$) and GRB20100612_T47056 ($\chi^2 = 2.2$). In both cases no excess in the count rate over the background level is detected in the softest KW channel (G1). The seven columns contain the following information: (1) the burst designation (see Table 1); columns (2) and (3) contain the spectrum start time T_{start} (relative to T_0) and its accumulation time (ΔT); (4) the spectral model; columns (5) and (6) contain α and E_p , respectively; (7) normalization (energy flux in the 10 keV–10 MeV band).

In Figure 3, we show the distributions for E_p and α . The low-energy indices α of the best-fit models for the multichannel spectra are distributed around a value of -0.5 . About 66% of the low-energy indices are $\alpha > -2/3$, violating the synchrotron “line-of-death” (Preece et al. 1998), while only 1% of the indices (three photon indices of the PL model) are $\alpha < -3/2$, violating the synchrotron cooling limit. For the four spectra that are best described with the PL model the photon indices are at the soft end of the low-energy index distribution. The high-energy indices are distributed around a slope $\beta = -2.3$. The E_p distribution for the CPL model peaks around 500 keV and covers just over two orders of magnitude. We studied the difference in the value of E_p between the BAND and CPL fits in the GOOD sample. We found that for each spectrum the E_p in the CPL and BAND models in the GOOD sample are consistent within 90% CL.

Three bright GRBs are found to have $P < 0.001$ for the fits of the time-integrated

spectra. We have explored these GRBs in more detail. In the case of GRB20060306_T55358, with $P \approx 10^{-4}$, the strong hard-to-soft evolution of the emission results in the poor BAND and CPL fits to the time-integrated spectrum. However, we found no strong deviation from the BAND model ($P > 0.05$) for the individual, time resolved spectra of this bright GRB. The time-integrated spectra of two other bursts, GRB19960908_T25028 and GRB20031214_T36655 turn out to be well described by a sum of CPL and PL functions. In addition, we found apparent systematics in the fit residuals for GRB19980205_T19785 ($P = 0.08$) whose spectrum is also well described by the CPL+PL combination. The parameters of the CPL+PL fits to time-integrated spectra of these GRBs are given in Table 5. For all three GRBs the PL component, which is also detected in most of the time resolved spectra of these bursts, is rather soft ($\alpha \sim -2$) and dominates the emission below ~ 50 – 100 keV. The hard CPL component is described by $E_p \sim (1.5$ – $2)$ MeV and considerably flatter photon index ($\alpha > -1$). All the above-mentioned GRBs are in the top 10% of the most intense ones in terms of their energy fluence, with GRB20031214_T36655 and GRB20060306_T55358 being the first and the second most intense bursts in our sample, respectively.

5.3. Fluences and peak fluxes

The values of S and F_{peak} were derived using the energy flux of the best-fit spectral model in the 10 keV–10 MeV band. Since the spectrum accumulation interval typically differs from the T_{100} interval a correction which accounts for the emission outside the time-integrated spectrum was introduced when calculating S . For short GRBs with EE, the energy fluences of the initial peak and EE were estimated separately (see also Section 5.4). F_{peak} was calculated on the 16 ms scale using the best-fit spectral model for the spectrum near the peak count rate. To obtain F_{peak} , the model energy flux was multiplied by the

ratio of the 16 ms peak count rate to the average count rate in the spectral accumulation interval. Typically, the corrections were made using counts in the G2+G3 light curve; the G1+G2, G2 only, and G1+G2+G3 combinations were also considered depending on the emission hardness and intensity.

Table 6 contains S and F_{peak} for the 293 bursts. The first column gives the burst designation (see Table 1). The three subsequent columns give S ; the start time of the 16-ms time interval, when the peak count rate in the G2+G3 band is reached; and F_{peak} . The distributions of S and F_{peak} are shown in Figure 4. The ranges of S and F_{peak} are $(0.2\text{--}140) \times 10^{-6} \text{ erg cm}^{-2}$ and $(0.2\text{--}85) \times 10^{-5} \text{ erg cm}^{-2} \text{ s}^{-1}$, respectively.

We note that for the handful of very intense, highly variable GRBs (i.e. GRB19970704_T04097, GRB20031214_T36655, GRB20051103_T33943, GRB20060306_T55358, GRB20070201_T55390, and GRB20070222_T27115) the values of F_{peak} (and to a lesser extent S) can be underestimated in our analysis by a factor of $\sim 1.5\text{--}2$, because the live time in a spectrum is estimated under the assumption of a constant count rate during the accumulation interval.

5.4. Short GRBs with extended emission

The extended emission (EE) component which follows the initial short pulse (IP) has been observed in a number of short GRBs by various experiments: *CGRO*-BATSE (Burenin 2000; Norris & Bonnell 2006; Bostancı et al. 2013), KW (Mazets et al. 2002; Frederiks et al. 2004), *INTEGRAL*-SPI-ACS (Minaev et al. 2010), *Swift*-BAT (Norris et al. 2011; Sakamoto et al. 2011b), and *Fermi*-GBM (Kaneke et al. 2015). We searched for candidates for short GRBs with EE in the full sample of 1939 *Konus-Wind* GRBs detected between 1994 and 2010. We defined the following search criteria: the burst initial pulse should

meet our criteria for a short GRB, i.e. have $T_{50} < 0.6$ s; and the remaining part of burst (EE) should not exhibit peaks with prominent spectral evolution. Applying these criteria to the full KW sample, we found 31 candidates for short GRBs with EE. Although the bright IP of GRB 070207 (Golenetskii et al. 2007) satisfies our criteria of a short GRB with $E_p \sim 300$ keV, the very intense and spectrally-hard ($E_p \sim 1.5$ MeV) behavior of the subsequent emission, which only formally can be considered as EE, suggests that this event is a long-duration, hard-spectrum burst with a short GRB-like precursor, very similar in morphology to two other KW bursts, GRB 000115 and GRB 001020.

Only for 21 of the remaining 30 events was the EE bright enough to allow spectral analysis. The initial pulses of these events are classified in Table 2 as Iee or Iee/II. Table 7 presents the parameters of the EE. The ten columns contain the following information: (1) the burst designation (see Table 1); columns (2) and (3) contain the EE start time (relative to T_0) and duration, determined at the 5σ confidence level in the G2 or G2+G1 bands; columns (4) and (5) contain the spectrum start time T_{start} (relative to T_0) and its accumulation time ΔT ; (6) best-fit models for each spectrum; (7) and (8) contain α and E_p ; (9) the EE energy fluence in the 10 keV–10 MeV band; (10) χ^2/dof along with the null hypothesis probability P .

In 15 cases EE is best fitted with PL and in six cases with the more complex CPL model. The PL indices range from -2.6 to -1.4 with a median of -1.6 , and the CPL photon indices range from -1.4 to -0.3 with a median of -1.2 . The E_p values range from ≈ 160 keV to ≈ 2.2 MeV with a median of ~ 300 keV and a geometric mean of 370 keV. For the 21 bursts, the fluence ratio, EE to initial pulse, ranges from 0.06 to 15 with a median of 3.3. Among six KW bursts whose EE can be well described with the CPL model, four have the E_p of the EE lower than that of the IP. Two bursts, GRB19950526_T16613 and GRB20090720_T61379, display EE harder than IP, with the latter having extremely hard

EE ($E_p = 2.2(-1.0, +2.4)$ MeV).

6. SUMMARY AND DISCUSSION

We have presented the results of the systematic spectral analysis of 293 short Konus-*Wind* GRBs, which is $\sim 15\%$ of all KW GRBs detected during the first fifteen years of operation. Among them, $\sim 70\%$ are classified as Type I bursts, $\sim 8\%$ as Type II, and $\sim 12\%$ have an uncertain type (I or II). The fraction of KW short GRBs that display extended emission is $\sim 10\%$.

In total we analyzed 253 multichannel spectra: 214 time-integrated spectra, 18 spectra near the peak count rate, and 21 spectra of the extended emission. We also analyzed 79 three-channel spectra. Table 8 contains the median values and 90% confidence intervals (CIs) for spectral parameter and energetics distributions resulting from our analysis. The first column gives the model name. The second gives the spectral data type: multichannel or three-channel. The subsequent ten columns contain median parameter values and 90% CI for α , β , E_p , S , and F_{peak} . The highest E_p found for KW short GRBs are ~ 3 MeV: $E_p = 3.55(-0.71, +0.85)$ MeV was observed in GRB20090510_T01381 (GRB 090510; Ackermann et al. 2010); just slightly softer are GRB19970704_T04097 and GRB20080611_T04742, both with $E_p \approx 3.3$ MeV. Almost all GRBs with $E_p \lesssim 200$ keV are classified as Type II or Type I/II and probably represent a population different from that of the harder GRBs (see the discussion below).

Our results support the previous findings that the spectra of the majority of short GRBs are well described by the CPL function with hard $\alpha \sim -0.5$ and E_p in the range of 100 keV–2 MeV. We found that the Band function is the best-fit model only for $\sim 4\%$ of KW short GRBs. Among the 5% highest- S GRBs 20% are best-fitted with BAND; the

remaining 80% of the bursts require a high-energy index $\beta \lesssim -2.5$ and in most cases are not constrained from below. This suggests that the absence of high-energy PL behavior observed in a large fraction of the bright short GRB spectra is likely intrinsic to the bursts rather than due to poor count statistics.

The scope of this catalog does not involve a study of the short GRB spectra with more complex models. Nevertheless, we found, that among the 214 bursts with multichannel spectra, three GRBs require an additional PL component with photon index of ~ -2 . These bursts belong to the brightest 10% of the sample. The ratio of the PL to CPL component energy flux ranges from 0.03 in GRB20031214.T366655 to 0.4 in GRB19980205.T19785. These PL components might be similar to that found for GRB 081024B (Abdo et al. 2010) and GRB 090510 (Ackermann et al. 2010) using *Fermi* GBM and LAT data. GRB 081024B was not detected by KW in the triggered mode while GRB 090510 (GRB20090510.T01381) is present in our sample. For the latter burst, the additional PL component is not needed to describe the KW time-integrated spectrum, and the estimated upper limit to the energy flux of the PL component with a photon index of -1.7 is $\sim 1 \times 10^{-6}$ erg cm $^{-2}$ s $^{-1}$ at 90% CL. The corresponding energy flux ratio, PL to BAND, is less than ~ 0.02 at 90% CL. A detailed study of the KW bursts with an additional spectral component will be published in a separate paper.

6.1. Comparison of KW with BATSE and GBM short GRBs

We compared the results of our spectral analysis to those reported for other instruments. The largest broadband GRB samples available to date are those reported by

CGRO-BATSE³ (20 keV–2 MeV; Goldstein et al. 2013) and *Fermi*-GBM⁴ (8 keV–40 MeV; Gruber et al. 2014). The present analysis contains about a factor of two more short GRBs than the GBM study, over a slightly narrower energy range, and a factor of ~ 1.5 less than the BATSE sample, but over a broader energy range.

From the BATSE 5B catalog we selected 427 bursts with $T_{90} < 2$ s and with the time-integrated spectrum accumulation interval being shorter than 10 s. Based on a $\Delta\chi^2 > 6$ criterion, the best-fit model statistics for these GRBs is: 11 — Band, 225 — CPL, and 191 — PL. From the GBM second catalog we selected 146 GRBs with $T_{90} < 2$ s. The best-fit models for the GBM bursts, as given in the catalog, are: 3 — Band, 67 — CPL, and 76 — PL; the bursts best described with smoothly broken power law were excluded from the comparison.

The ratio of Band to CPL best-fit models is small ($\lesssim 5\%$) for all samples. We tested whether distributions of α and E_p of the CPL model are consistent between the instruments. The two-sided p-values of the two-sample Kolmogorov-Smirnov test (P_{KS}) for KW and GBM α and E_p distributions are 10% and 25%, respectively, while for KW and BATSE, and GBM and BATSE $P_{KS} < 1\%$. The BATSE sample has median $\alpha = -0.33$ while medians for KW and GBM are $\alpha = -0.49$ and $\alpha = -0.50$, respectively. The median of the E_p distribution is ~ 400 keV for BATSE and ~ 550 keV for both KW and GBM. Thus, the KW results are consistent with GBM and to a slightly lesser extent with BATSE.

The fractions of best-fit PL models in each sample are: 2% (5% using $\Delta\chi^2 > 6$ criterion) — KW, 52% — GBM, 55% — BATSE. We have investigated the origin of a high fraction of PLs in the BATSE and GBM samples. To make the comparison more robust,

³<http://heasarc.gsfc.nasa.gov/W3Browse/cgro/bat5bgrbsp.html>

⁴<http://heasarc.gsfc.nasa.gov/W3Browse/fermi/fermigbrst.html>

we selected the bursts with $S > 5.5 \times 10^{-7}$ erg cm $^{-2}$, which is approximately the lowest S measured for KW short GRBs with multichannel spectra. The resulted subsamples of 138 (BATSE) and 49 (GBM) GRBs contain 29 (21%) and 3 (6%) PLs, respectively. Thus, in the common fluence range, the fractions of best-fit PLs for KW and GBM are consistent. Among GOOD CPL models for the 29 BATSE bursts 17 have 1σ upper limits of E_p not constrained to the upper BATSE spectral band boundary (2 MeV). The remaining 12 bursts represent 9% of the subsample. Thus, the main source of the relatively high PL fractions in the BATSE and GBM short GRBs samples is a large amount of weak bursts for which a more complex model cannot be preferred due to low count statistics. Also, for the BATSE bursts the additional bias toward the PLs comes from the relatively narrow energy band.

6.2. Extended emission

We found that 30 bursts from the sample of 1939 KW GRBs detected from 1994 to 2010 can be classified as short GRBs with EE based on the short duration of an initial pulse and the presence of subsequent emission exhibiting no prominent spectral evolution. Of them 21 GRBs have intense enough EE to perform spectral analysis. For six KW bursts the EE spectrum requires a “curved” (CPL) model with rather high $E_p \sim 160$ keV–2.2 MeV. The IPs of two of them are classified as Iee/II and they are probably long GRBs with a short initial pulse. The four remaining events, however, are “canonical” short/hard GRBs with EE in terms of the light curve shape. Similar EE spectral behavior was reported earlier for two out of 19 BATSE GRBs (Bostancı et al. 2013) and for four out of 14 GBM bursts (Kaneko et al. 2015); our results provide additional evidence of rather hard EE being observed in some short GRBs.

In total, our sample contains two short GRBs with EE detected by BATSE and three EE bursts detected by GBM. The comparison of the fits shows that the EE

spectral parameters for these bursts, including those for one common GRB with hard EE (GRB20090831_T27393; $E_p \approx 215$ keV), are consistent within errors between KW and the other instruments. The KW GRB20090720_T61379 showing extremely hard EE ($E_p \approx 2.2$ MeV) was also detected by GBM. Although this burst had not been included by Kaneko et al. (2015) in the EE sample, the GBM time-integrated spectral parameters (Gruber et al. 2014) are consistent with the KW fits we made for the same time interval.

The bright, nearby GRB 060614, which can be regarded as a short GRB with EE (Gehrels et al. 2006), was detected by KW ($T_0(\text{KW})=45831.590$ s; Golenetskii et al. 2006), but was not included in our short GRBs sample because of the long duration of the initial peak $T_{50} = 2.7 \pm 0.3$ s.

6.3. Giant flare candidates

The enormous initial pulse of a soft gamma-repeater giant flare (GF) can mimic a classical short GRB even when observed from a nearby galaxy. An upper limit on the fraction of such events among observed short GRBs was estimated in several studies to be $\sim 1\text{--}15\%$, see Hurley (2011) for a review. Svinkin et al. (2015) performed a search for GFs in the KW short GRB sample using the burst localizations from Pal'shin et al. (2013). Only two earlier reported candidates were found, GRB 051103 (GRB20051103_T33943) in the M81/M82 group of galaxies (Frederiks et al. 2007) and GRB 070201 (GRB20070201_T55390) in the Andromeda galaxy (Mazets et al. 2008). Both GRB 051103 and GRB 070201 are in the 10% of the most intense bursts in terms of total energy fluence, while GRB 051103 is the brightest in terms of the peak energy flux. The spectral parameters of the bursts are typical for our sample. A count excess observed up to 90 s after trigger for GRB 070201 was suggested by Mazets et al. (2008) to be the tail of the possible GF. The significance of the

excess is 4.3σ and it does not meet our 5σ EE criterion.

6.4. Heterogeneity of short GRBs

Figure 5 shows E_p of the CPL best-fit model as a function of the burst duration T_{50} . The Type I GRBs tend to be harder ($E_p \gtrsim 200$ keV) and shorter than Type II bursts, which is consistent with the classification obtained using the hardness-duration distribution. Among four bursts best-fitted with the PL model, two are types I and II, and two have uncertain classifications (I/II). The apparent lack of KW GRBs with $E_p \lesssim 100$ keV and $T_{50} \lesssim 0.3$ s is probably due to selection effects. The duration distribution of the initial pulses of short GRBs with EE (Iee) is consistent with that of the Type I bursts; this is supported by $P_{KS} \sim 0.5$. We found that the E_p of the initial pulses of Iee bursts are, on average, harder than the E_p of the Type I bursts by a factor of ~ 1.5 , and P_{KS} for the two E_p distributions is ~ 0.01 . Finally, we tested whether the S and F_{peak} distributions for the initial peaks of the Iee bursts differ from those of Type I GRBs. In both cases we obtained $P_{KS} \sim 0.01$ which disfavors the hypothesis that both Iee and Type I GRBs are drawn from the same population, with short GRBs with EE being, on average, more intense.

Figure 6 shows E_p as a function of S and F_{peak} . The 79 faint bursts, for which only three-channel spectra were available for the analysis, show spectral parameter and F_{peak} distributions similar to those of more fluent GRBs from the sample; also, these bursts smoothly extend the short-hard (Type I) GRB distribution to the low- S region in the E_p - S plane. The candidate for a GF in the Andromeda galaxy (GRB 070201) is an apparent outlier in the E_p - F_{peak} distribution, supporting the non-GRB nature of this event. Type I and Type II bursts occupy virtually non-overlapping regions in the E_p - S plane. The Type I GRBs form an elongated distribution that generally follows an $E_p \propto S^{1/2}$ relation. The Type II bursts from our sample do not share this correlation; they form a small,

soft-spectrum population which represents a tiny fragment of the long-soft KW GRB distribution. To a lesser extent, the same is true of the Type I and Type II population behavior in the E_p – F_{peak} plane. Since only nine bursts from our sample have known redshift ($z \sim 0.1$ – 1.0 , determined either spectroscopically or photometrically), the rest-frame properties of the bursts are not discussed in this work. The detailed analysis of all KW GRBs with known redshifts will be presented in a separate paper (Tsvetkova et al., in prep.). Although the instrumental biases affect the burst sample properties, the correlations in the observer frame may still be the consequences of the rest-frame $E_{\text{p,rest}}$ – E_{iso} (Amati et al. 2002) and $E_{\text{p,rest}}$ – L_{iso} (Yonetoku et al. 2004) correlations (see, e.g., Nava et al. 2008 and references therein). Thus, the properties of the observer-frame hardness-intensity distribution obtained for Type I and Type II bursts from the KW short GRB sample favor the hypothesis that short/hard GRBs follow their own form of the “Amati” $E_{\text{p,rest}}$ – E_{iso} relation (see, e.g., Nava et al. 2011 and references therein).

Figure 7 shows $\log N$ – $\log S$ and $\log N$ – $\log F_{\text{peak}}$ distributions for 293 KW short GRBs along with a homogeneous space distribution with index $-3/2$. The $\log N$ – $\log S$ distribution tends to follow this slope only in a limited range of fluences, $(\sim 4\text{--}10) \times 10^{-6}$ erg cm $^{-2}$. While the deficit of the faint bursts can be explained by instrumental bias, the visible excess of intense bursts is, to a significant extent, due to events not representing the “classical” short/hard GRB population. Among the 12 most energetic GRBs in our sample, with $S \gtrsim 2 \times 10^{-5}$ erg cm $^{-2}$, only four are of Type I; the others are Type I/II, Type II, or bursts with EE (Iee). After all non-Type I GRBs are excluded from the consideration, the $\log N$ – $\log S$ distribution shows a good agreement with a steep slope of -1.85 ± 0.30 above $S \sim 5 \times 10^{-6}$ erg cm $^{-2}$. The $\log N$ – $\log F_{\text{peak}}$ distribution of the KW short GRBs is also more shallow than the $-3/2$ slope; we estimate the power-law index of the integral distribution to be -1.16 ± 0.12 for F_{peak} in the $(0.2\text{--}9.4) \times 10^{-4}$ erg cm $^{-2}$ s $^{-1}$ range. In the same range, the $\log N$ – $\log F_{\text{peak}}$ distribution of Type I bursts demonstrates a steeper slope

of -1.42 ± 0.16 , in agreement with the homogenous distribution.

Plots of the KW short GRBs time histories and spectral fits can be found at the Ioffe Web site⁵. We note that KW continues to operate well, and has detected ~ 380 short bursts up to December 2015. The results of the analyses of the short GRBs detected by *Konus-Wind* after 2010 will be presented on-line at the same URL.

We thank the reviewer comments which significantly contributed to improving the quality of the publication. R.L.A. and S.V.G. gratefully acknowledge support from RFBR grants 15-02-00532 and 13-02-12017-ofi-m. This research made use of Astropy⁶, a community-developed core Python package for Astronomy (Astropy Collaboration et al. 2013).

Facilities: *Wind* (Konus).

⁵<http://www.ioffe.ru/LEA/shortGRBs/Catalog2/>

⁶<http://www.astropy.org>

REFERENCES

- Abdo, A. A., Ackermann, M., Ajello, M., et al. 2010, *ApJ*, 712, 558
- Ackermann, M., Asano, K., Atwood, W. B., et al. 2010, *ApJ*, 716, 1178
- Agostinelli, S., Allison, J., Amako, K., et al. 2003, *Nuclear Instruments and Methods in Physics Research A*, 506, 250
- Amati, L., Frontera, F., Tavani, M., et al. 2002, *A&A*, 390, 81
- Aptekar, R. L., Frederiks, D. D., Golenetskii, S. V., et al. 1995, *Space Sci. Rev.*, 71, 265
- Arnaud, K. A. 1996, in *Astronomical Society of the Pacific Conference Series*, Vol. 101, *Astronomical Data Analysis Software and Systems V*, ed. G. H. Jacoby & J. Barnes, 17
- Astropy Collaboration, Robitaille, T. P., Tollerud, E. J., et al. 2013, *A&A*, 558, A33
- Band, D., Matteson, J., Ford, L., et al. 1993, *ApJ*, 413, 281
- Berger, E. 2014, *ARA&A*, 52, 43
- Bostancı, Z. F., Kaneko, Y., & Göğüş, E. 2013, *MNRAS*, 428, 1623
- Burenin, R. A. 2000, *Astr. Lett.*, 26, 269
- Frederiks, D. D., Aptekar, R. L., Golenetskii, S. V., et al. 2004, in *Astronomical Society of the Pacific Conference Series*, Vol. 312, *Gamma-Ray Bursts in the Afterglow Era*, ed. M. Feroci, F. Frontera, N. Masetti, & L. Piro, 197
- Frederiks, D. D., Pal’shin, V. D., Aptekar, R. L., et al. 2007, *Astronomy Letters*, 33, 19
- Gehrels, N., Norris, J. P., Barthelmy, S. D., et al. 2006, *Nature*, 444, 1044

- Goldstein, A., Preece, R. D., Mallozzi, R. S., et al. 2013, *ApJS*, 208, 21
- Golenetskii, S., Aptekar, R., Mazets, E., et al. 2006, *GRB Coordinates Network*, 5264, 1
- . 2007, *GRB Coordinates Network*, 6089
- Gruber, D., Goldstein, A., Weller von Ahlefeld, V., et al. 2014, *ApJS*, 211, 12
- Horváth, I., Bagoly, Z., Balázs, L. G., et al. 2010, *ApJ*, 713, 552
- Hurley, K. 2011, *Advances in Space Research*, 47, 1337
- Hurley, K., Mitrofanov, I. G., Golovin, D., et al. 2013, in *EAS Publications Series*, Vol. 61, *EAS Publications Series*, ed. A. J. Castro-Tirado, J. Gorosabel, & I. H. Park, 459–464
- Kaneko, Y., Bostancı, Z. F., Göğüş, E., & Lin, L. 2015, *MNRAS*, 452, 824
- Kouveliotou, C., Meegan, C. A., Fishman, G. J., et al. 1993, *ApJ*, 413, L101
- Krimm, H. A., Hurkett, C., Pal’shin, V., et al. 2006, *ApJ*, 648, 1117
- Lipunov, V. M., Gorosabel, J., Pruzhinskaya, M. V., et al. 2016, *MNRAS*, 455, 712
- Mazets, E. P., Aptekar, R. L., Frederiks, D. D., et al. 2002, *ArXiv Astrophysics e-prints*, astro-ph/0209219
- Mazets, E. P., Cline, T. L., Aptekar, R. L., et al. 1999, *Astronomy Letters*, 25, 635
- Mazets, E. P., Golenetskii, S. V., Ilinskii, V. N., et al. 1981, *Ap&SS*, 80, 3
- Mazets, E. P., Aptekar, R. L., Cline, T. L., et al. 2008, *ApJ*, 680, 545
- Minaev, P. Y., Pozanenko, A. S., & Loznikov, V. M. 2010, *Astr. Lett.*, 36, 707
- Nava, L., Ghirlanda, G., Ghisellini, G., & Celotti, A. 2011, *MNRAS*, 415, 3153

- Nava, L., Ghirlanda, G., Ghisellini, G., & Firmani, C. 2008, *MNRAS*, 391, 639
- Norris, J. P., & Bonnell, J. T. 2006, *ApJ*, 643, 266
- Norris, J. P., Gehrels, N., & Scargle, J. D. 2011, *ApJ*, 735, 23
- Norris, J. P., Marani, G. F., & Bonnell, J. T. 2000, *ApJ*, 534, 248
- Norris, J. P., Scargle, J. D., & Bonnell, J. T. 2001, in *Gamma-ray Bursts in the Afterglow Era*, ed. E. Costa, F. Frontera, & J. Hjorth, 40
- Pal’shin, V. D., Hurley, K., Svinkin, D. S., et al. 2013, *ApJS*, 207, 38
- Preece, R. D., Briggs, M. S., Mallozzi, R. S., et al. 1998, *ApJ*, 506, L23
- Roming, P. W. A., Vanden Berk, D., Pal’shin, V., et al. 2006, *ApJ*, 651, 985
- Sakamoto, T., Pal’shin, V., Yamaoka, K., et al. 2011a, *PASJ*, 63, 215
- Sakamoto, T., Barthelmy, S. D., Baumgartner, W. H., et al. 2011b, *ApJS*, 195, 2
- Starling, R. L. C., Rol, E., van der Horst, A. J., et al. 2009, *MNRAS*, 400, 90
- Svinkin, D. S., Hurley, K., Aptekar, R. L., Golenetskii, S. V., & Frederiks, D. D. 2015, *MNRAS*, 447, 1028
- Terekhov, M. M., Aptekar, R. L., Frederiks, D. D., et al. 1998, in *American Institute of Physics Conference Series*, Vol. 428, *Gamma-Ray Bursts*, 4th Hunstville Symposium, ed. C. A. Meegan, R. D. Preece, & T. M. Koshut, 894–898
- Yonetoku, D., Murakami, T., Nakamura, T., et al. 2004, *ApJ*, 609, 935
- Zhang, B., Zhang, B.-B., Virgili, F. J., et al. 2009, *ApJ*, 703, 1696

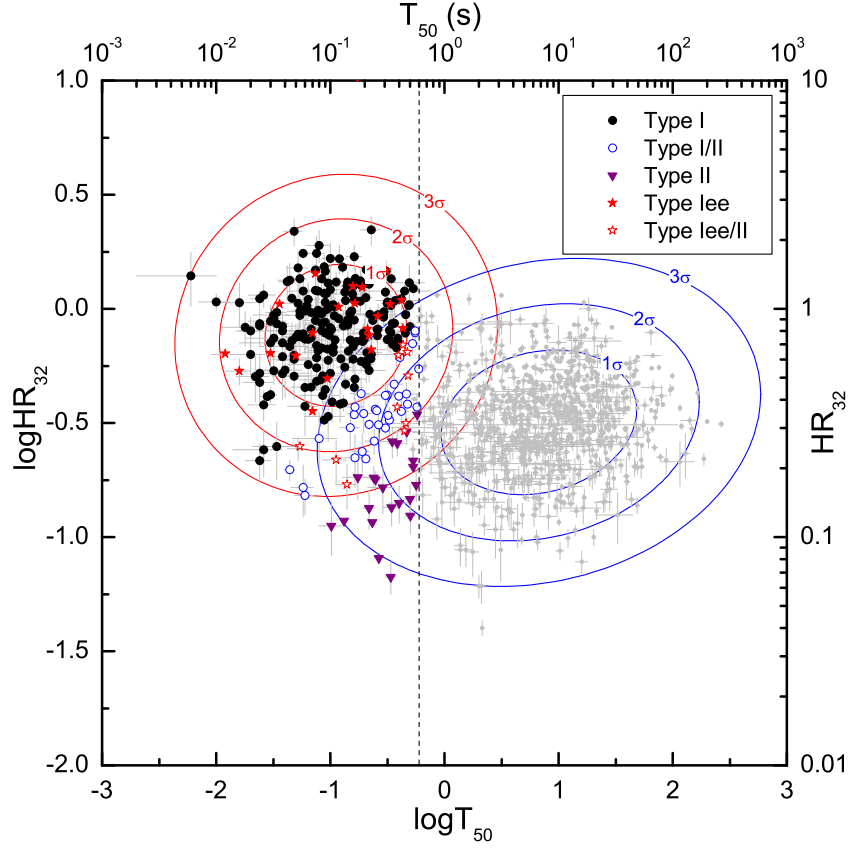


Fig. 1.— Hardness-duration distribution of 1143 Konus-*Wind* bright GRBs. The distribution is fitted by a sum of two Gaussian distributions using the expectation and maximization (EM) algorithm. The contours denote 1σ , 2σ , and 3σ confidence regions for each Gaussian distribution. The vertical dashed line denotes the boundary ($T_{50} = 0.6$ s) between long and short KW GRBs. The types for GRBs with $T_{50} < 0.6$ s are shown in colors.

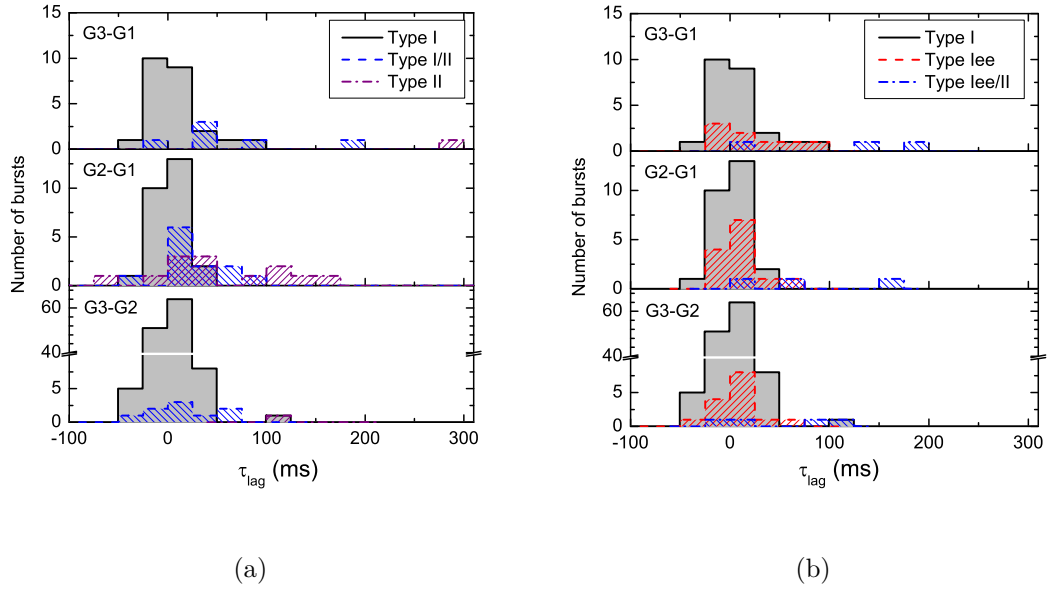


Fig. 2.— Spectral lag distributions of short KW GRBs without (a) and with EE (b). Panel (a) shows: Type I bursts (gray filled histogram), Type I/II bursts (dashed histogram), and Type II bursts (dash-dotted histogram). Panel (b) shows: Type I bursts (gray filled histogram), Type Iee bursts (dashed histogram), and Type Iee/II bursts (dash-dotted histogram).

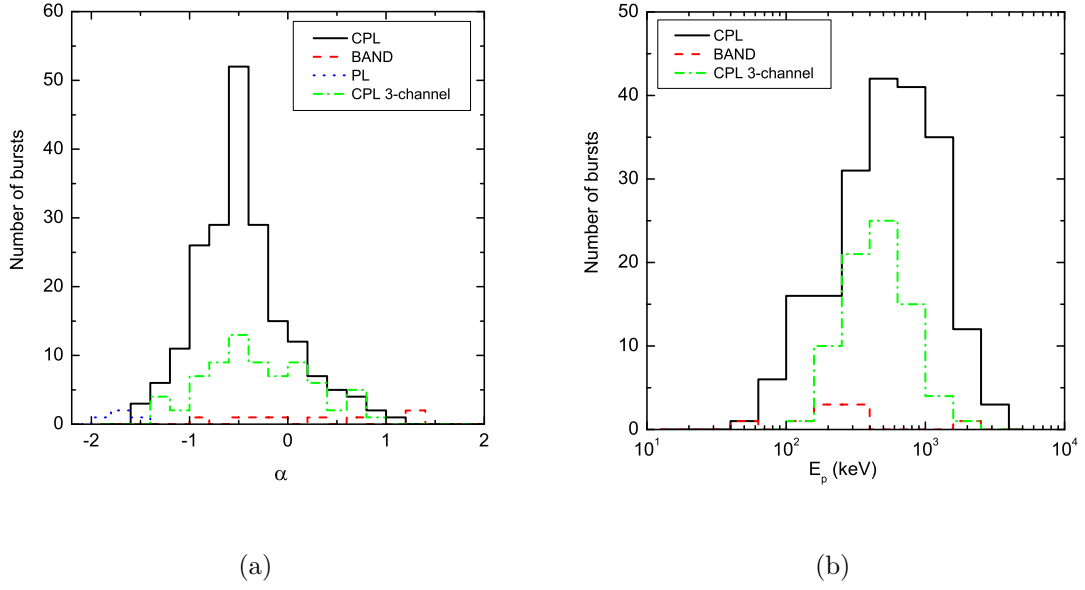


Fig. 3.— Distributions of α (a) and E_p (b) obtained from time-integrated spectral fits with different models, shown in colors.

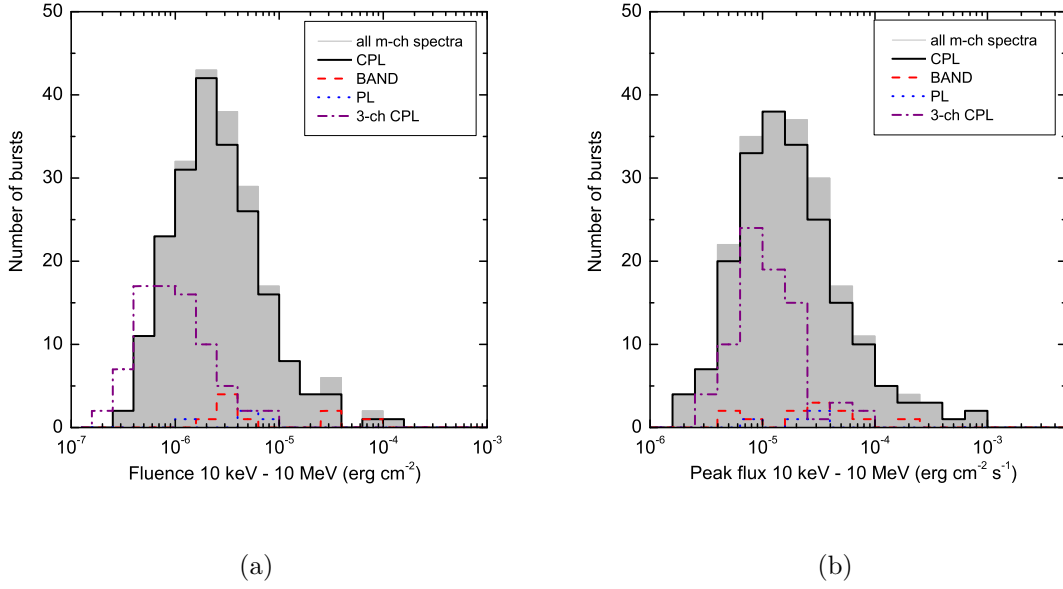


Fig. 4.— Distributions of the total energy fluence (a) and the peak energy flux (b). The gray filled histogram in each panel shows the total distribution for 214 multichannel spectra and the constituents are shown in color. The dash-dotted histograms show distributions for 79 three-channel spectra.

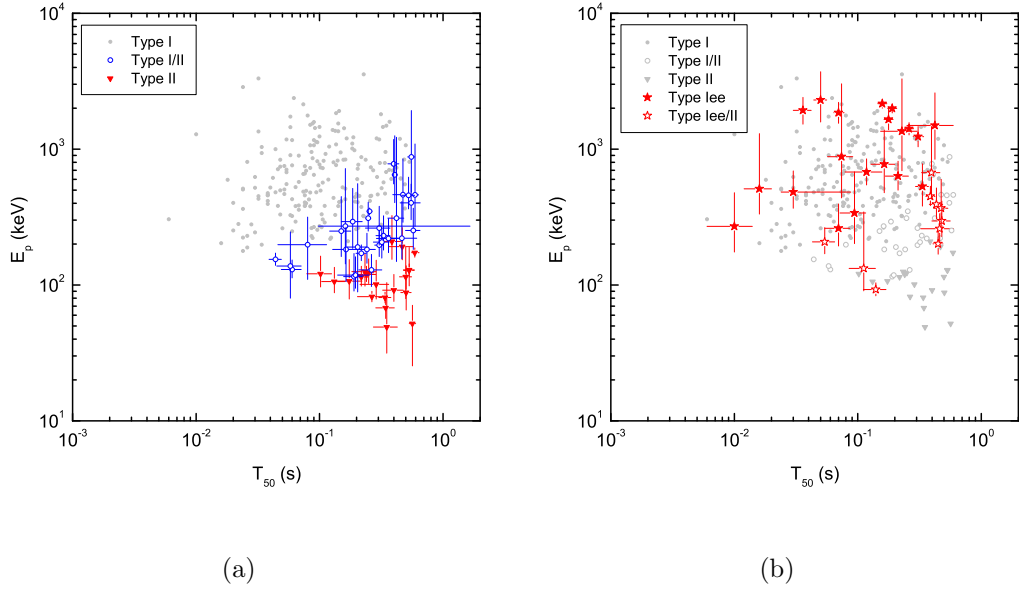


Fig. 5.— Best-fit model E_p as a function of T_{50} (only CPL fits are shown). Panel (a) shows Type I bursts (gray dots), Type II bursts (red triangles), and bursts of uncertain type, I or II (blue circles). Panel (b) shows the Type I bursts with EE (filled red stars), and bursts of uncertain type, Iee or II (empty stars). For Type I GRBs error bars are not shown.

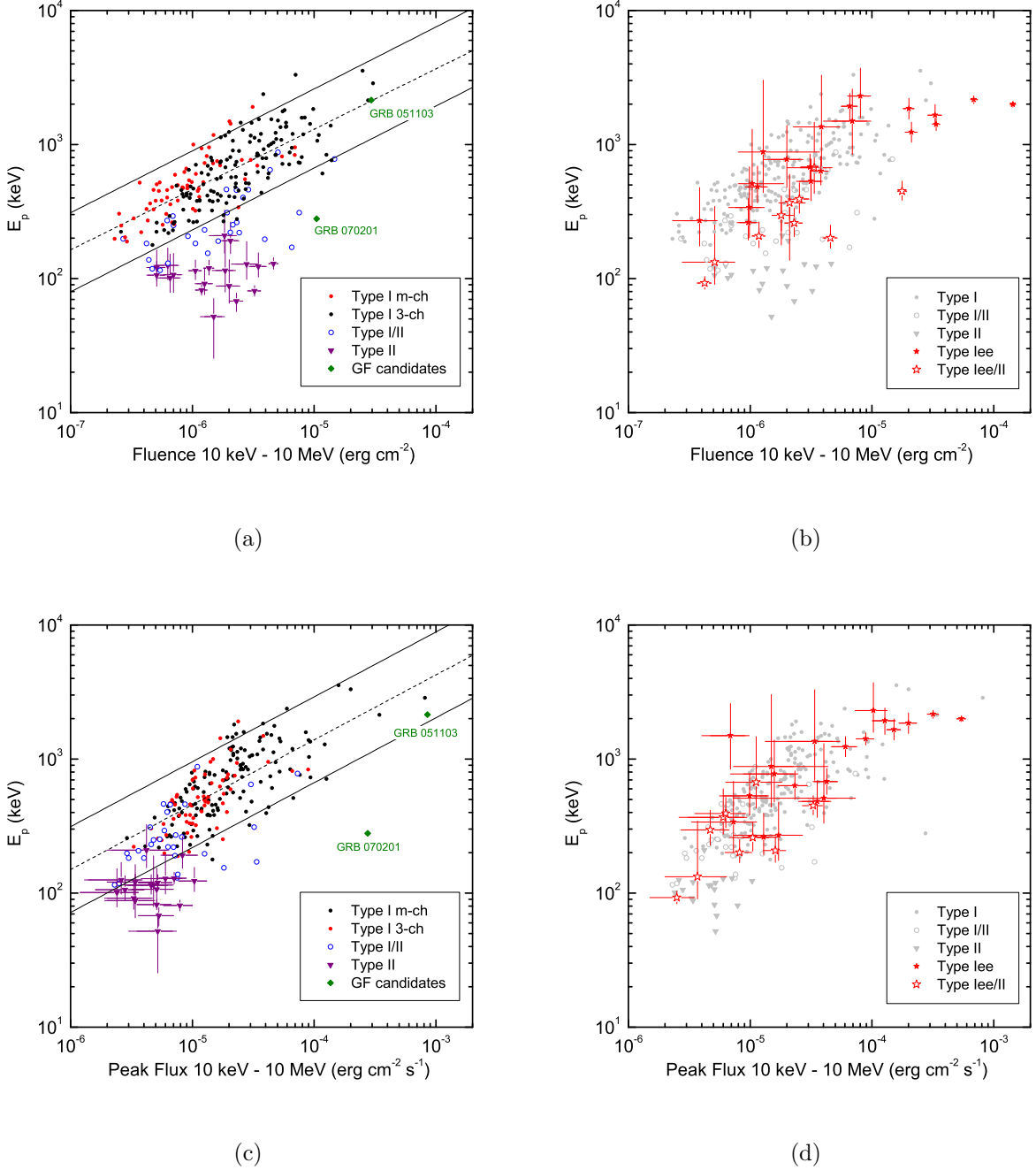


Fig. 6.— E_p as a function of the total energy fluence and the peak energy flux for the best CPL fits. Panel (a) shows E_p vs. the total energy fluence distribution for the Type I bursts with multichannel spectra (black circles); the Type I bursts with three-channel spectra (red circles); the bursts with uncertain type (empty circles), for both types of spectra; and the Type II bursts (triangles). Panel (b) shows bursts of types Iee (filled stars) and Iee/II (empty stars); the remaining bursts from the sample are shown in gray. Panels (c) and (d) show E_p vs. the peak energy flux distribution for the same GRB groups. For the GRBs of type I and I/II error bars are not shown. The extragalactic SGR giant flare candidates are shown with diamonds. The dashed lines denote the best powerlaw fits for the E_p - S (with an index of 0.46 ± 0.16) and E_p - F_{peak} (with an index of 0.48 ± 0.18) relations of the Type I GRBs. The solid lines denote the 90% prediction bands.

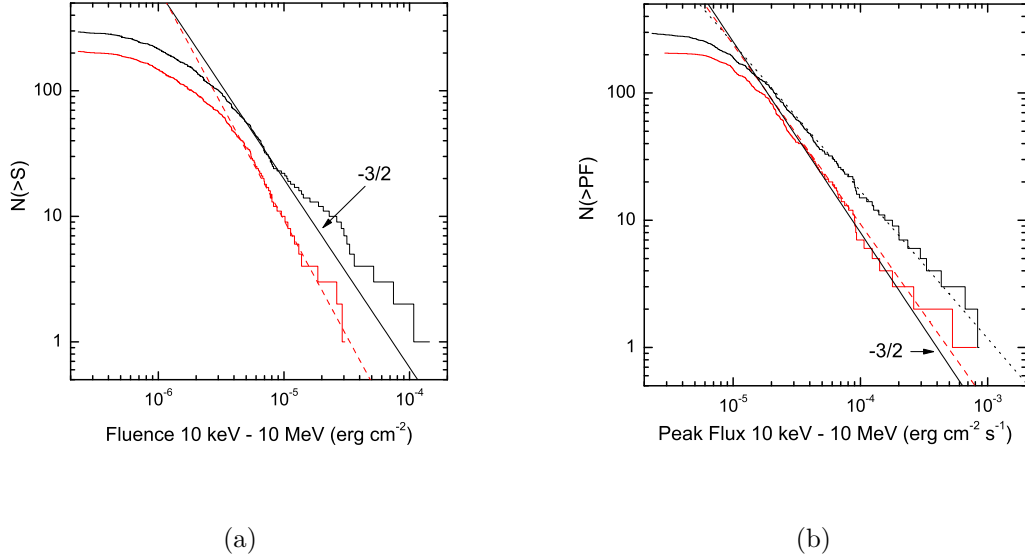


Fig. 7.— Cumulative distributions of the total energy fluence (left panel) and the peak energy flux (right panel). In both panels upper (black) and lower (red) histograms represent the distributions built for the whole short GRB sample and for the Type I GRB sub-sample, respectively. The dashed lines and dotted lines show the best power-law approximations to the corresponding distributions (see Section 6 for the approximation ranges and the indices). The solid lines show a slope of $-3/2$ expected if GRBs were homogeneously distributed in an Euclidean space throughout the sampled volume.

Table 1. Konus-*Wind* short GRB observation details

Designation	Konus- <i>Wind</i> Trigger Time (UT)	Name ^a	Detector	Incident angle ($^{\circ}$)	Comment ^b
GRB19950210_T08424	02:20:24.147	...	S1	55(-0,+0)	2
GRB19950211_T08697	02:24:57.748	...	S2	47(-0,+0)	2
GRB19950414_T40882	11:21:22.798	...	S1	57(-57,+30)	5
GRB19950503_T66971	18:36:11.838	...	S1	73(-0,+0)	2
GRB19950520_T83271	23:07:51.403	...	S1	46(-46,+30)	5

^aas provided in the GCN circulars, if available

^b1 — detected by imaging instruments (incident angle error is not given); 2 — burst localized to a box or segment, localization center is used; 3 — burst localized to a box or segment, ecliptic latitude estimate is used; 4 — burst localized to a single annulus, a position on the annulus center line which is the most consistent with the ecliptic latitude estimate is used; 5 — observed by Konus-*Wind* only, ecliptic latitude estimate is used.

Note. — (This table is available in its entirety in a machine-readable form in the online journal. A portion is shown here for guidance regarding its form and content.)

Table 2. Durations, spectral lags, and classification

Designation	t_0^a (s)	T_{100} (s)	T_{50} (s)	T_{90} (s)	Type	$\tau_{\text{lag}32}$ (ms)	$\tau_{\text{lag}31}$ (ms)	$\tau_{\text{lag}21}$ (ms)
GRB19950210_T08424	-0.034	0.176	0.060 ± 0.011	0.138 ± 0.024	I/II
GRB19950211_T08697	-0.046	0.214	0.030 ± 0.004	0.104 ± 0.030	I	12 ± 2	22 ± 10	18 ± 8
GRB19950414_T40882	-0.130	0.164	0.048 ± 0.020	0.150 ± 0.014	I	6 ± 10
GRB19950503_T66971	-0.206	0.402	0.050 ± 0.006	0.282 ± 0.049	Iee	-1 ± 3	...	-1 ± 14
GRB19950520_T83271	-0.162	1.218	0.210 ± 0.073	1.100 ± 0.219	I	1 ± 13
GRB19950526_T16613	-0.510	1.934	0.480 ± 0.081	1.464 ± 0.377	Iee/II

^aRelative to the trigger time

Table 3. Spectral parameters (multichannel spectra)

Designation	Spec. Type	$T_{\text{start}}^{\text{a}}$ (s)	ΔT (s)	Model ^b	α	β	E_{p} (keV)	Flux norm. (10^{-6} erg cm $^{-2}$ s $^{-1}$)	χ^2/dof (Prob.)
GRB19950210_T0842	i,p	0.0	0.128	CPL*	$-0.01(-0.48, +0.62)$	\dots	$130(-17, +23)$	$3.7(-0.5, +0.5)$	7/17 (0.978)
				BAND	$0.14(-0.58, +0.93)$	$-3.37(-6.63, +0.80)$	$123(-23, +26)$	$4.1(-0.8, +1.2)$	7/16 (0.979)
GRB19950211_T0869	i,p	0.0	0.128	CPL	$-0.54(-0.18, +0.22)$	\dots	$346(-59, +78)$	$15.5(-1.9, +2.1)$	32/29 (0.311)
				BAND*	$-0.22(-0.30, +0.40)$	$-2.28(-0.45, +0.23)$	$244(-52, +75)$	$22.0(-4.4, +4.8)$	24/28 (0.701)
GRB19950503_T6697	i,p	0.0	0.128	PL	$-1.30(-0.05, +0.05)$	\dots	\dots	$77.1(-10.5, +11.0)$	40/28 (0.060)
				CPL*	$-1.05(-0.11, +0.12)$	\dots	$2298(-716, +1413)$	$48.4(-10.2, +12.6)$	21/27 (0.786)
GRB19950520_T8327	i,p	0.0	0.192	PL	$-1.35(-0.09, +0.09)$	\dots	\dots	$11.0(-3.1, +3.4)$	36/21 (0.024)
				CPL*	$-0.46(-0.42, +0.56)$	\dots	$452(-147, +358)$	$3.2(-0.9, +1.5)$	13/20 (0.878)
				BAND	$-0.40(-0.44, +8.62)$	$-2.38(-7.62, +0.81)$	$410(-292, +317)$	$4.5(-2.1, +5.0)$	12/19 (0.876)
GRB19950805_T1345	i,p	0.0	0.064	PL	$-1.21(-0.06, +0.06)$	\dots	\dots	$68.0(-13.2, +14.2)$	31/15 (0.009)
				CPL*	$-0.84(-0.16, +0.21)$	\dots	$1123(-424, +792)$	$25.0(-7.1, +10.1)$	10/14 (0.752)
				BAND	$-0.51(-0.39, +0.71)$	$-1.65(-1.38, +0.23)$	$418(-240, +793)$	$40.8(-16.4, +16.0)$	7/13 (0.889)

^aRelative to the trigger time

^bThe best-fit model is indicated by the asterisk

Note. — (This table is available in its entirety in a machine-readable form in the online journal. A portion is shown here for guidance regarding its form and content.)

Table 4. Spectral parameters (three-channel spectra)

Designation	$T_{\text{start}}^{\text{a}}$ (s)	ΔT^{b} (s)	Model	α	E_{p} (keV)	Flux (10^{-6} erg cm $^{-2}$ s $^{-1}$)
GRB19950414_T40882	-0.130	0.164	CPL	$-0.52(-0.51, +1.03)$	$497(-206, +2440)$	$4.6(-1.4, +9.8)$
GRB19950526_T16613	-0.510	1.918	CPL	$0.32(-0.68, +1.94)$	$296(-68, +118)$	$0.9(-0.2, +0.2)$
GRB19950610_T19096	-0.052	0.110	CPL	$0.72(-0.71, +1.46)$	$189(-30, +45)$	$2.7(-0.4, +0.6)$
GRB19951013_T57097	-0.030	0.052	CPL	$3.96(-3.72, +6.04)$	$252(-50, +170)$	$11.0(-1.9, +4.4)$
GRB19960312_T35074	-0.156	0.208	CPL	$0.24(-0.62, +1.29)$	$222(-45, +90)$	$1.8(-0.3, +0.5)$

^ais the burst start time t_0

^bis the burst total duration T_{100}

Note. — (This table is available in its entirety in a machine-readable form in the online journal. A portion is shown here for guidance regarding its form and content.)

Table 5. Parameters of CPL+PL model fits

Designation	α_{CPL}	$E_{\text{p,CPL}}$ (keV)	Flux $_{\text{CPL}}^{\text{a}}$	α_{PL}	Flux $_{\text{PL}}^{\text{a}}$	χ^2/dof (Prob.)
GRB19960908_T25028	$-0.48(-0.47, +0.84)$	$1528(-282, +357)$	$27.3(-8.0, +7.0)$	$-2.07(-0.42, +0.23)$	$8.7(-5.2, +8.8)$	77/63 (0.11)
GRB19980205_T19785	$-0.70(-0.60, +1.20)$	$1812(-672, +1333)$	$13.2(-5.6, +6.2)$	$-2.22(-0.50, +0.24)$	$5.4(-3.0, +3.9)$	40/55 (0.94)
GRB20031214_T36655	$-0.31(-0.10, +0.11)$	$1912(-83, +81)$	$274.6(-13.4, +12.4)$	$-2.01(-0.39, +0.20)$	$10.6(-5.6, +8.6)$	87/75 (0.15)

^aIn units of 10^{-6} erg cm $^{-2}$

Table 6. Fluences and Peak Fluxes

Designation	Fluence (10^{-6} erg cm $^{-2}$)	T_{pk} (s)	Peak Flux (10^{-5} erg cm $^{-2}$ s $^{-1}$)
GRB19950210_T08424	0.63(-0.07,+0.08)	-0.004	0.75(-0.18,+0.18)
GRB19950211_T08697	3.26(-0.58,+0.63)	0.014	6.16(-1.37,+1.48)
GRB19950414_T40882	0.76(-0.23,+1.61)	-0.036	1.25(-0.49,+2.67)
GRB19950503_T66971	8.03(-1.40,+1.72)	0.034	10.30(-2.57,+3.03)
GRB19950520_T83271	1.42(-0.33,+0.50)	0.018	1.00(-0.38,+0.53)

Note. — (This table is available in its entirety in a machine-readable form in the online journal. A portion is shown here for guidance regarding its form and content.)

Table 7. Short GRBs with EE

Designation	EE t_0^a	EE T_{100}	T_{start}	ΔT	Best-fit	α	E_p	Fluence	χ^2/dof
	(s)	(s)	(s)	(s)	Model		(keV)	(10^{-6} erg cm $^{-2}$)	(Prob.)
GRB19950503_T66971	6.288	109.936	0.256	78.848	CPL	$-1.61(-0.11, +0.12)$	$157(-24, +39)$	$41.6(-3.0, +3.9)$	100/75 (0.03)
GRB19950526_T16613	28.192	64.032	41.216	23.552	CPL	$-1.15(-0.13, +0.15)$	$489(-125, +230)$	$13.6(-1.9, +2.6)$	74/76 (0.54)
GRB19961225_T36436	14.784	12.176	8.448	24.576	PL	$-1.57(-0.14, +0.16)$...	$17.1(-5.6, +7.4)$	74/74 (0.47)
GRB19970625_T23681	19.152	16.752
GRB19970923_T41961	27.136	29.056	24.832	32.768	PL	$-1.47(-0.29, +0.30)$...	$8.3(-5.2, +10.0)$	90/65 (0.02)
GRB19980605_T51131	2.160	111.760
GRB19980706_T57586	1.392	24.560
GRB19981107_T00781	2.816	16.480	8.704	24.576	PL	$-1.49(-0.27, +0.28)$...	$9.5(-4.7, +7.8)$	42/72 (1.00)
GRB19981218_T62134 ^b	45.760	3.776
GRB19990313_T33712	2.048	70.976	8.448	65.536	PL	$-1.90(-0.30, +0.41)$...	$4.4(-2.2, +4.6)$	42/63 (0.98)
GRB19990327_T22911	1.136	61.328	0.256	16.384	CPL	$-1.18(-0.19, +0.23)$	$389(-111, +244)$	$11.2(-1.8, +2.6)$	84/62 (0.03)
GRB19990516_T86065	1.408	94.016	8.448	24.576	PL	$-1.85(-0.12, +0.13)$...	$18.2(-3.7, +4.5)$	52/64 (0.86)
GRB19990712_T27915	6.320	34.256	8.448	32.768	PL	$-2.33(-0.24, +0.28)$...	$5.2(-1.0, +1.4)$	69/63 (0.27)
GRB20000218_T58744	2.400	61.344	5.888	72.960	PL	$-1.60(-0.08, +0.08)$...	$80.1(-12.8, +15.3)$	71/63 (0.23)
GRB20010317_T23290	25.376	27.744	25.344	8.192	CPL	$-0.29(-0.98, +1.73)$	$181(-46, +93)$	$2.4(-0.6, +0.8)$	67/52 (0.08)
GRB20030105_T52454	39.360	72.000	41.216	65.536	PL	$-2.58(-0.47, +0.71)$...	$2.4(-0.8, +1.3)$	46/60 (0.91)
GRB20031214_T36655	2.000	70.128	8.704	65.536	PL	$-1.92(-0.39, +0.46)$...	$8.2(-3.3, +7.2)$	51/61 (0.82)
GRB20040210_T40272	2.016	6.032
GRB20040816_T29998	8.048	52.752	8.448	57.344	PL	$-1.76(-0.17, +0.18)$...	$16.4(-5.3, +7.8)$	53/60 (0.72)
GRB20050513_T16804	6.048	7.520
GRB20060228_T44827	6.240	47.584	8.448	49.152	PL	$-1.61(-0.14, +0.15)$...	$21.4(-6.5, +8.9)$	60/59 (0.44)
GRB20061006_T60326	8.960	160.768	8.448	73.728	PL	$-1.38(-0.38, +0.44)$...	$19.0(-11.8, +23.5)$	59/59 (0.46)

Table 7—Continued

Designation	EE t_0^a (s)	EE T_{100} (s)	T_{start} (s)	ΔT (s)	Best-fit Model	α	E_p (keV)	Fluence (10^{-6} erg cm $^{-2}$)	χ^2/dof (Prob.)
GRB20070915_T30890	2.096	54.480
GRB20071030_T31964	39.744	60.608
GRB20080807_T85828	3.952	16.080	8.448	16.384	PL	$-1.53(-0.13, +0.14)$...	$18.9(-4.6, +6.0)$	64/65 (0.49)
GRB20090525_T18274	9.296	46.768	8.448	49.152	PL	$-1.72(-0.12, +0.12)$...	$15.5(-4.4, +5.8)$	55/59 (0.63)
GRB20090720_T61379	2.176	14.080	0.256	8.192	CPL	$-1.30(-0.10, +0.11)$	$2250(-1076, +2418)$	$16.4(-4.4, +5.1)$	94/97 (0.56)
GRB20090831_T27393	3.312	80.848	0.256	40.96	CPL	$-1.42(-0.16, +0.18)$	$215(-48, +93)$	$14.4(-1.7, +2.2)$	66/61 (0.31)
GRB20100714_T59238	10.720	137.248
GRB20100916_T67270	9.520	12.768	8.448	8.192	PL	$-1.58(-0.30, +0.36)$...	$3.2(-1.7, +3.2)$	86/58 (0.01)

^aRelative to the trigger time^bThere is a solar flare in the data at $\sim T_0 + 100$ s

Table 8. Best-fit model parameter distributions

Model	Data Type ^a	Number of Spectra	α		β		E_p (keV)		Fluence ^b		Peak Flux ^c	
			Median	CI	Median	CI	Median	CI	Median	CI	Median	CI
PL	mult	4	−1.78	[−1.99, −1.61]	4.1	[1.4, 5.7]	2.1	[0.8, 3.0]
CPL	mult	201	−0.47	[−1.14, 0.52]	563	[115, 1807]	2.3	[0.5, 13.9]	1.5	[0.3, 12.8]
BAND	mult	9	−0.12	[−1.13, 1.42]	−2.28	[−3.15, −1.74]	204	[40, 364]	3.8	[1.9, 39.1]	2.8	[0.5, 7.3]
	all	214	2.4	[0.5, 20.1]	1.6	[0.4, 12.8]
CPL	3ch	79	−0.36	[−1.23, 0.90]	459	[190, 1180]	0.9	[0.3, 3.4]	1.0	[0.4, 4.0]

^aMultichannel spectrum — “mult” or three-channel spectrum — “3ch”

^bIn units of 10^{-6} erg cm $^{-2}$

^cIn units of 10^{-5} erg cm $^{-2}$ s $^{-1}$